Electronic Supporting Information

N, S-codoped carbon microporous structure derived from dead ginkgo leaves as an efficient oxygen reduction reaction catalysts for Al-air Batteries

Kun Liu[a], Angli Zhang[a], Xiaowu Liu[a], Ting Liang[a], Xin Li[a], Ke Hu[a], Fanqing Ji[a], Haoyi Li [a], Xin Chen[a*], Xucheng Fu[b *]

[a] *Anhui Provincial Laboratory of Biomimetic Sensor and Detecting Technology, College of Materials and Chemical Engineering, West Anhui University, Lu'an 237012, Anhui Province, China.*

[b] *Analytical and Testing Center, West Anhui University, Lu'an 237012, Anhui Province, China.*

Electrochemical measurements

The treated sample (4mg) was dispersed in a mixture of 950 μL ethanol and 100 μL Nafion solution with a concentration of 5wt%. Ultrasonic treatment was conducted for 30 minutes to achieve uniform dispersion of the ink. The above mixture is applied onto a glass carbon electrode with a diameter of 5mm, serving as the working electrode in the three-electrode system after drying. The reference electrode [Hg/HgO] and counter electrode (platinum wire) are also included. Before each test, a 0.1M KOH electrolyte is injected and saturated by bubbling high purity oxygen or nitrogen for 30 minutes. The ORR electrochemical activity of the samples was investigated at room temperature using a rotating ring electrode (RRDE) at the Ivium electrochemical station. The electrochemical tests are conducted within the voltage range of -1.0 to 0.2 V, unless otherwise specified, with a scan rate of 10 mV⓾s^{-1} for data collection purposes. The normalized catalyst area (expressed as $mA \cdot cm^{-2}$) was obtained based on the current data for comparative analysis of oxygen reduction performance. The optimized catalyst was subjected to 5000 cycles in an O_2-saturated 0.1M KOH solution, with a

scanning rate of 50 $mV \cdot s^{-1}$ within the potential range of 0.6~1.2 V, in order to assess its long-term durability.

The Koutecky-Levich diagrams (J^{-1} vs $\omega^{-1/2}$) were investigated at various electrode potentials. The Koutecky-Levich equation enables the determination of oxygen reduction electron transfer number (n) by calculating the slope of its linear regression line. The kinetic properties of the prepared samples can be assessed using the following Koutecky-Levich equation:[1-3]

$$\frac{1}{j} = \frac{1}{j_L} + \frac{1}{j_K} = \frac{1}{B\omega^{1/2}} + \frac{1}{j_K} \quad \text{Equation (1)}$$

$$B = 0.62nFC_0D_0^{2/3}\upsilon^{-1/6} \quad \text{Equation (2)}$$

For the Tafel plot, the kinetic current was calculated as equation (3):

$$j_K = \frac{j \times j_L}{j_L - j} \quad \text{Equation (3)}$$

The experimentally determined current density, labeled as j, is compared against both the diffusional-limited current density (j_L) and dynamic current density (j_K). The rotational speed of the electrode is denoted as ω in radians per second. F denotes the Faraday constant at a value of 96485 $C \cdot mol^{-1}$. Additionally, C_0 corresponds to the volume concentration of O_2 in 0.1 M KOH at a magnitude of $1.2 \times 10^{-3} mol \cdot L^{-1}$, while D_0 represents its diffusion coefficient at a rate of 1.9×10^{-5} $cm^2 \cdot s^{-1}$. Furthermore, ν signifies the kinematic viscosity of the electrolyte with an assigned value equaling 0.01 $cm^2 \cdot S^{-1}$.

The rotating ring disk electrode (RRDE) technique was employed to determine the transfer number (n), providing values for both the electron transfer number (n) and hydrogen peroxide yield ($\%H_2O_2$) in the formula as follows:

$$\%HO_2^- = 200 \times \frac{I_r / N}{I_d + I_r / N} \quad (4)$$

$$n = 4 \times \frac{I_d}{I_d + I_r / N} \quad (5)$$

Where I_d represents disk current, I_r represents ring current, and N represents current collection

efficiency of the Pt ring (0.424).

The electrochemical surface area (ECSA) of the prepared catalyst was assessed through cyclic voltammetry (CV) in a non-rotating N_2-saturated 0.1M KOH electrolyte. CV curves were recorded for RDE working electrodes at various scanning rates (1, 2, 5, 10, 15, 20 and 25 mV/s) within the non-faradic potential range of 1.00~1.10V relative to RHE. Subsequently, a scatter plot was generated depicting the average current density (ΔJ/2, ΔJ = Ja-Jc, mA/cm^2) against sweep rate (mV/s) at 1.05V. The slope obtained from linear regression analysis between ΔJ/2 and scan rate corresponds to the differential capacitance value (C_{dl}, mF/cm^2), which is directly proportional to ECSA and can be utilized for comparing ECSA among different materials，ECSA = $\frac{C_{dl}}{C_s}$, the ECSA can be calculated. Here, C_s = 0.04 mF/cm^2, which is the speciffc capacitance.[4-6]

The mass activity (MA) is calculated by following equation:[7]

$$MA\ (mA\ mg^{-1}) = J_k \times \frac{area}{mass\ of\ catalyst} \quad (6)$$

where J_k is the kinetic current density (mA/cm^2) and area is the geometric area of working electrode (0.1257 cm^2). The mass activity of the catalyst is estimated via the calculation of J_k and normalization to the catalyst loading on glassy carbon rotating disk electrode.

The specific activity (SA) is calculated by following equation:[8]

$$\text{SA (mA cm}^{-2}) = \frac{i_k}{Ar} \quad (7)$$

$$i_k = \frac{i_{lim} \times i}{i_{lim} - i} \quad (8)$$

where i is the measured current at a specified potential, $i_{lim}$is the measured limiting current, i_k is the kinetic current and Ar real surface area.

Fabrication and performance evaluation of Al-air batteries

A three-layer air electrode, comprising a gas diffusion layer, a flow collecting layer, and a catalytic layer, was fabricated using the hot pressing method. The discharge stability of the catalyst in an aluminum-air battery was investigated. Nickel foam is utilized as an excellent conductor for air electrodes.The catalyst is uniformly blended with Ketjenblack, acetylene black, and polytetrafluoroethylene (PTFE) in a weight ratio of 3:3:1:3. The mixture is then dispersed into a

homogeneous slurry, continuously ground until it reaches a paste-like consistency. Subsequently, the resulting paste is applied onto a glass plate and rolled out to approximately 0.2 mm thickness to form the catalytic layer. The thickness of the air electrode was compressed using the roller press (MSK-HRp-MR100A) provided by Hefei Kejing. Finally, the catalytic layer sample should be dried overnight in a vacuum at 80°C. Throughout the battery testing process, the catalytic layer acts as the cathode, while the polished aluminum alloy electrode acts as the anode. The electrochemical corrosion inhibition mechanism of aluminum-air batteries was investigated using a 6M KOH electrolyte containing Na_2SnO_3, ZnO and $In(OH)_3$. The constant discharge test was conducted using the Neware battery test system manufactured in Shenzhen, China. The battery discharge test was performed with OMS-TF1, an aluminum-air battery testing device developed by Changzhou Youcott New Energy Technology Co., LTD.

Supporting Figures

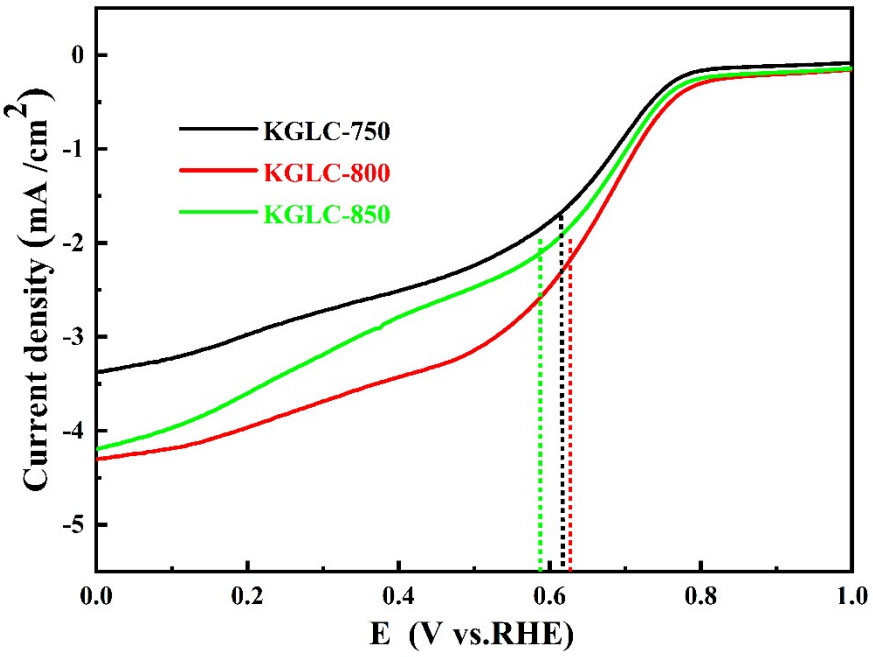

Figure S1. LSV curves of activated carbon samples for different calcination temperatures

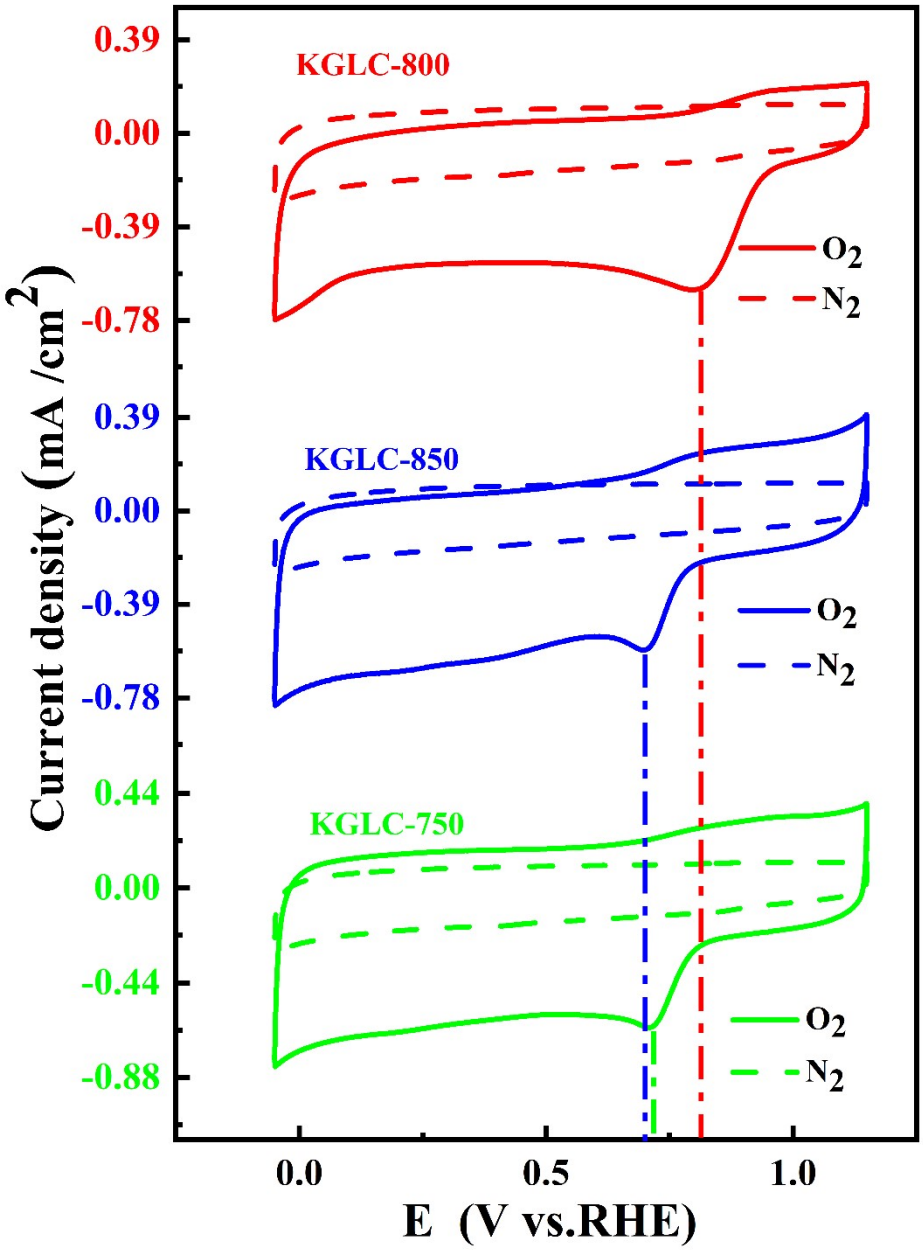

Figure S2. CV curves of activated carbon samples for different calcination temperatures in O_2-saturated (solid line) and N_2-saturated (dash line) electrolyte.

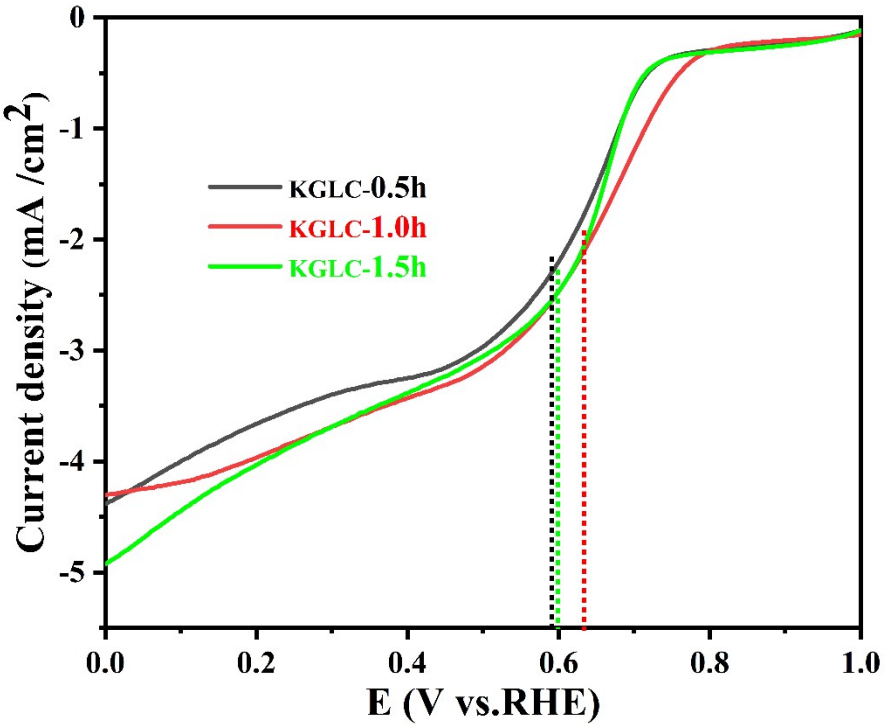

Figure S3. LSV curves of activated carbon samples for different calcination times.

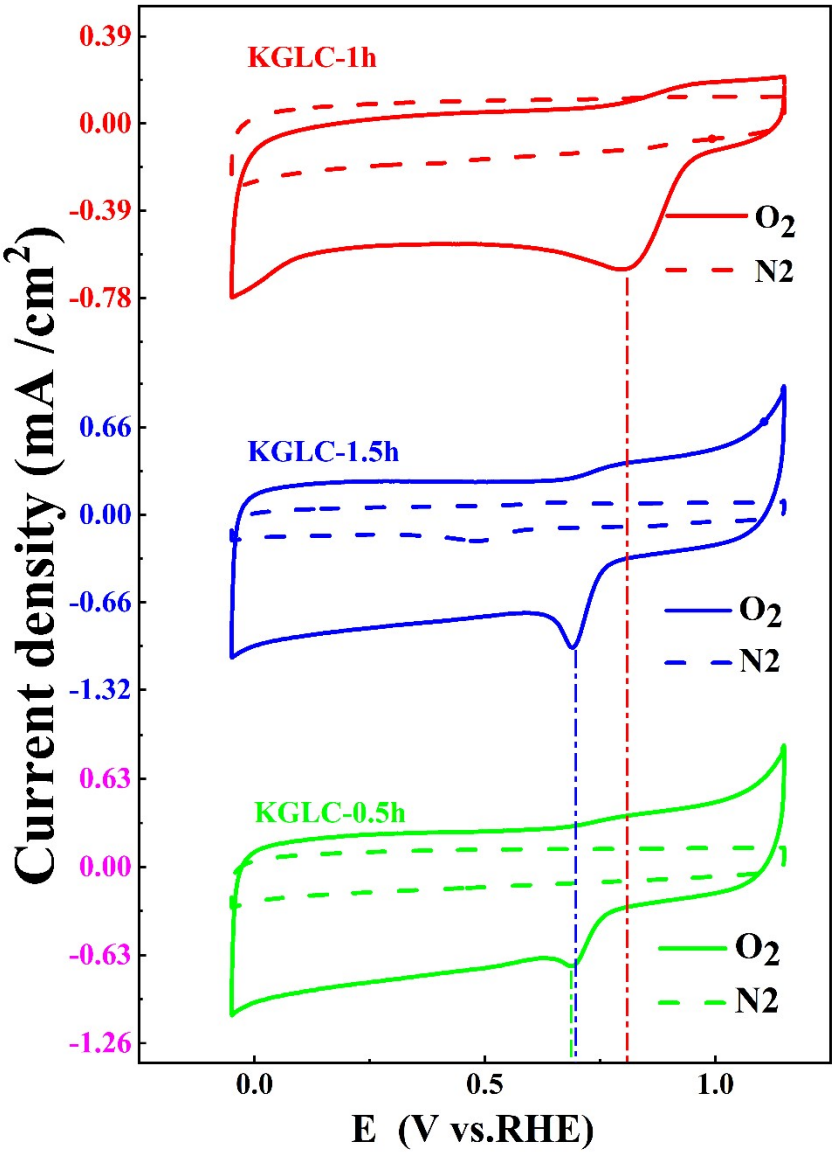

Figure S4. CV curves of activated carbon samples for different calcination times in O_2-saturated (solid line) and N_2-saturated (dash line) electrolyte.

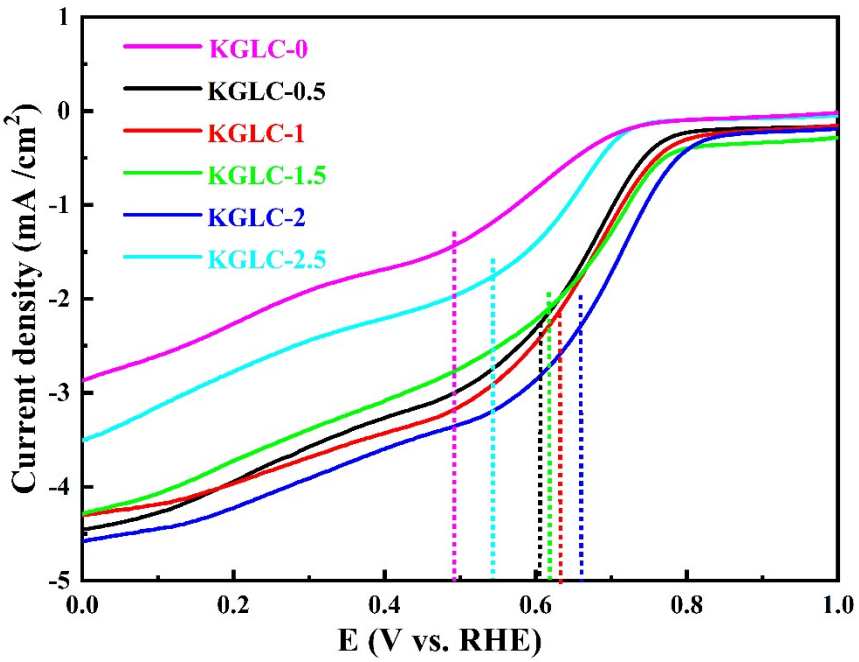

Figure S5. LSV curves of activated carbon samples for different mass ratios of KOH to pretreatment carbon.

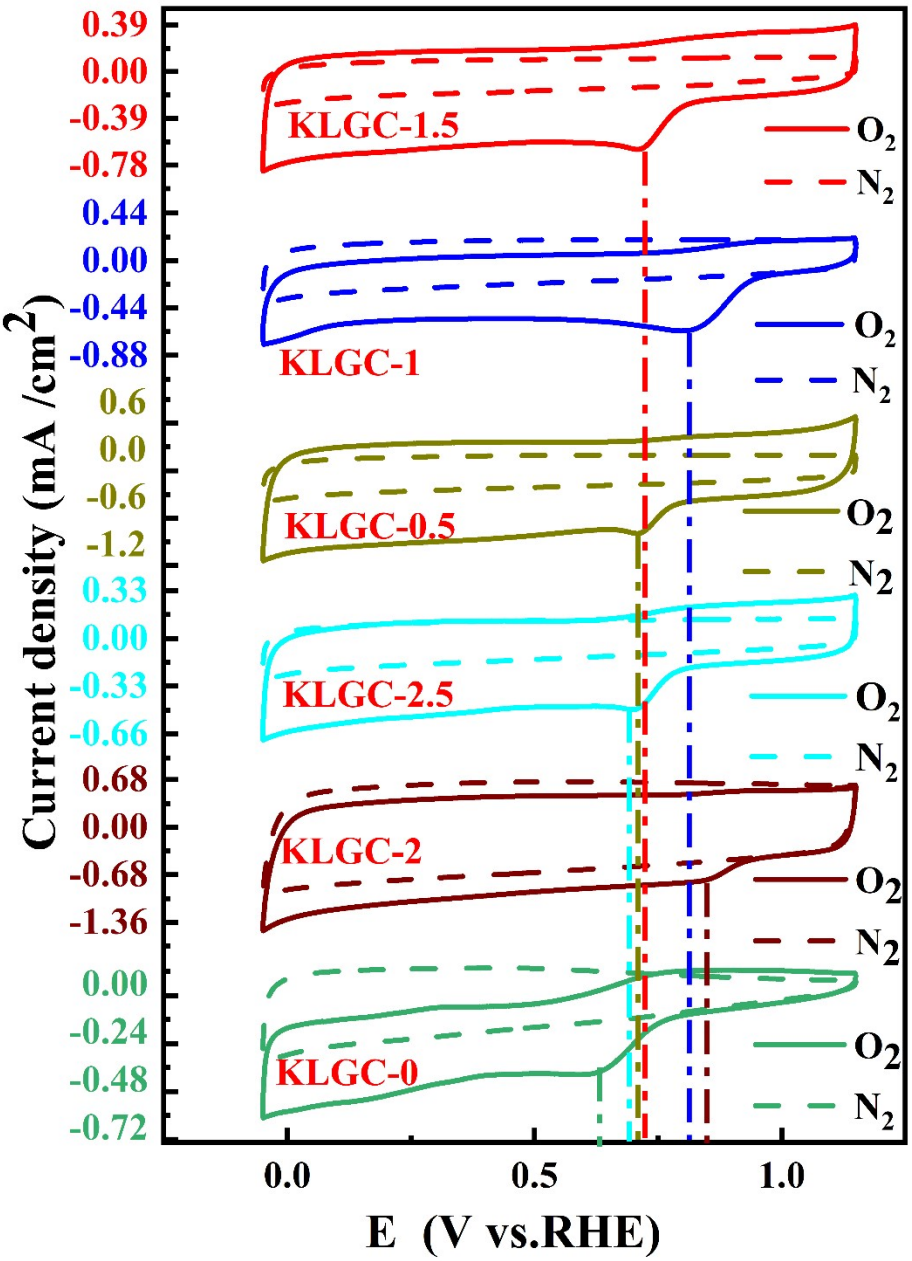

Figure S6. CV curves of activated carbon samples for different mass ratios of KOH to pretreatment carbon in O_2-saturated (solid line) and N_2-saturated (dash line) electrolyte.

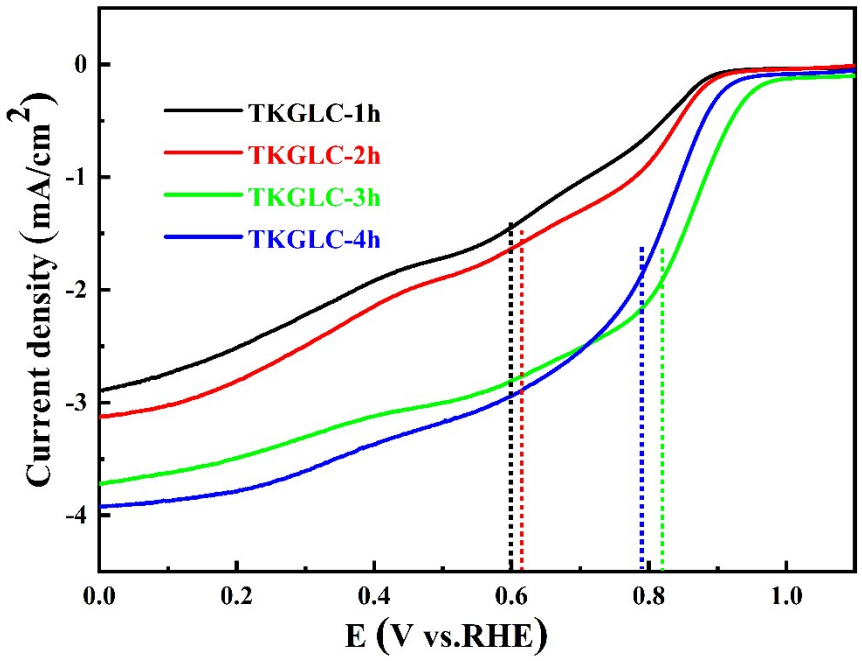

Figure S7. LSV curves of N, S co-doped carbon samples for different calcination times.

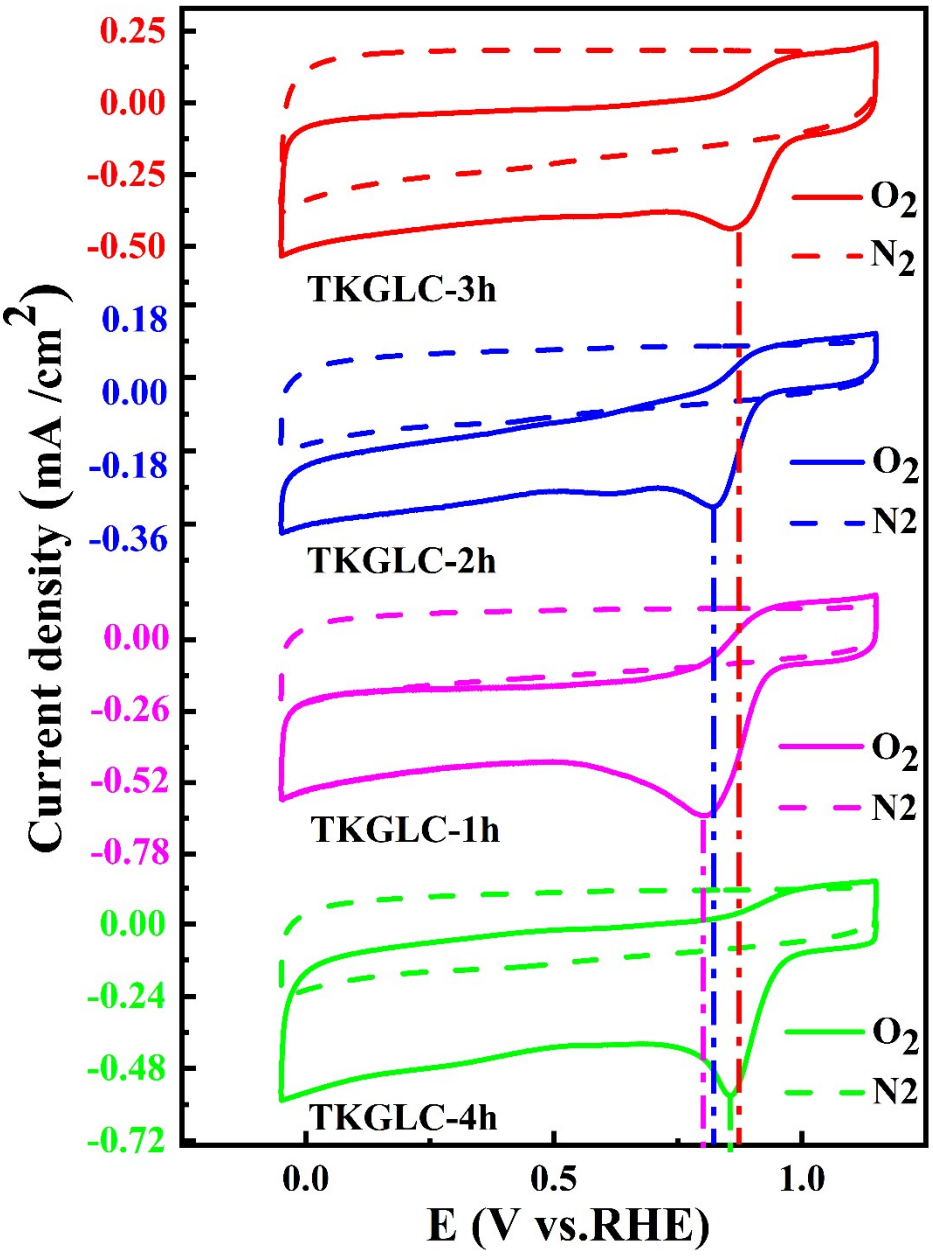

Figure S8. CV curves of N, S co-doped carbon samples for different calcination times in O_2-saturated (solid line) and N_2-saturated (dash line) electrolyte.

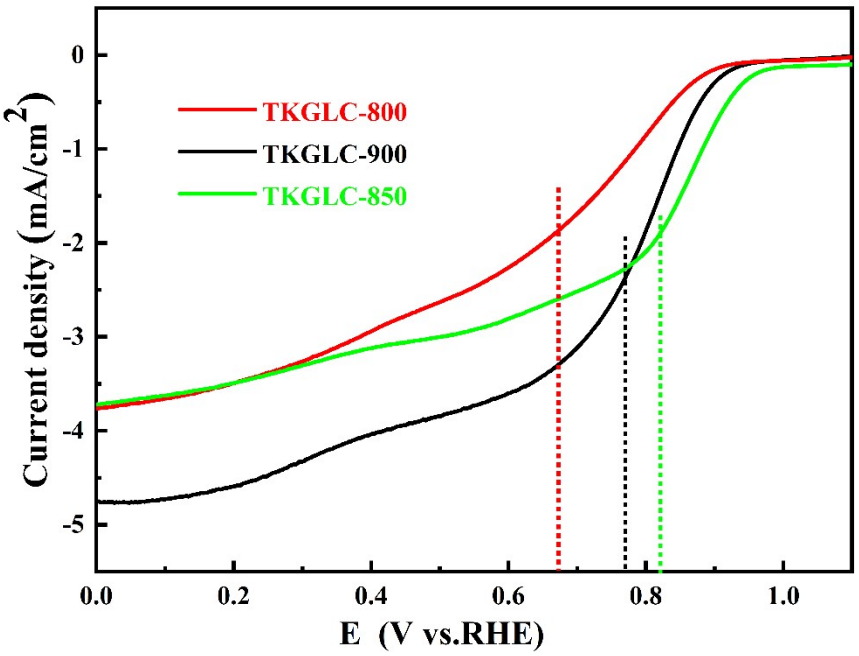

Figure S9. LSV curves of N, S co-doped carbon samples for different calcination temperatures.

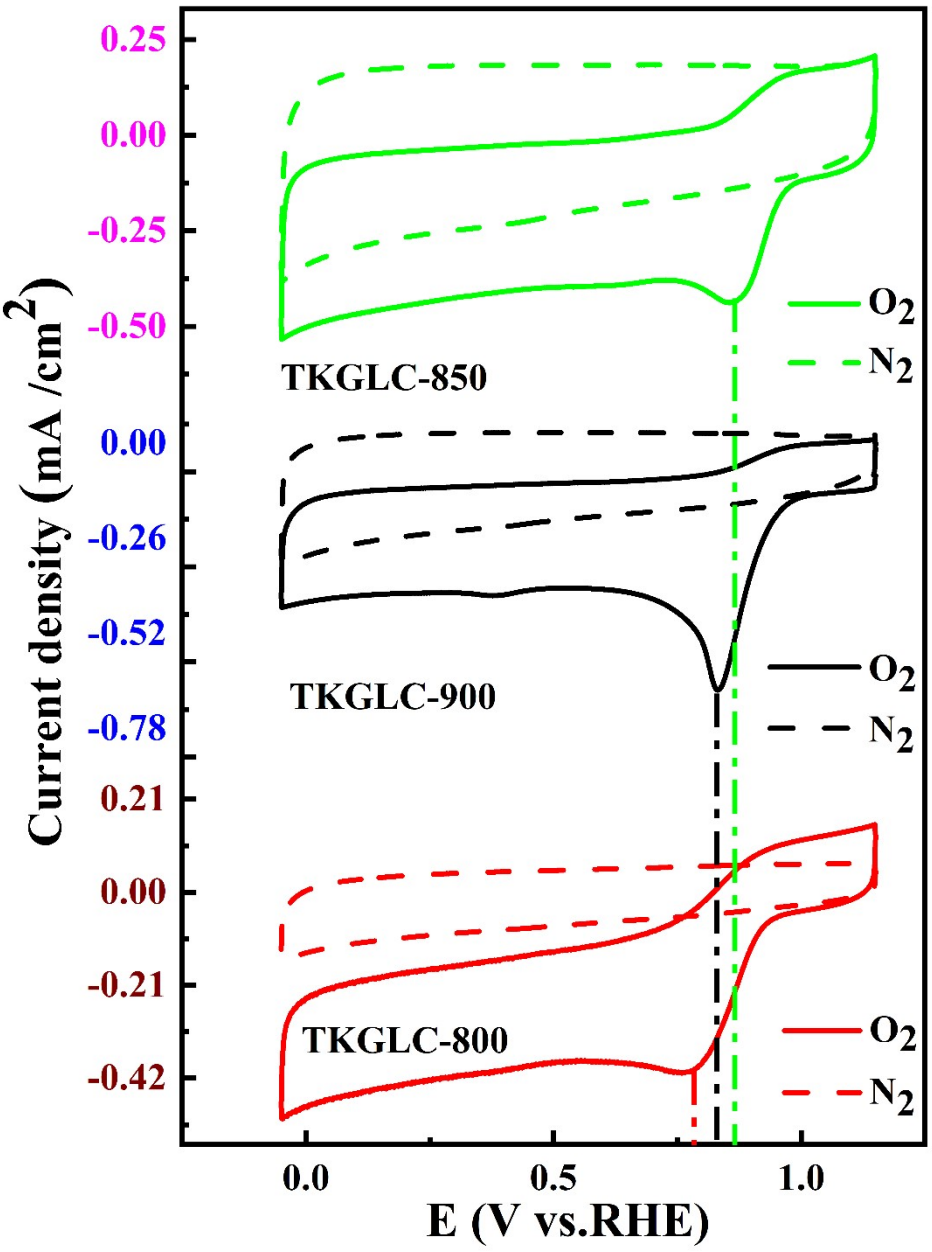

Figure S10. CV curves of N, S co-doped carbon samples for different calcination temperatures in O_2-saturated (solid line) and N_2-saturated (dash line) electrolyte.

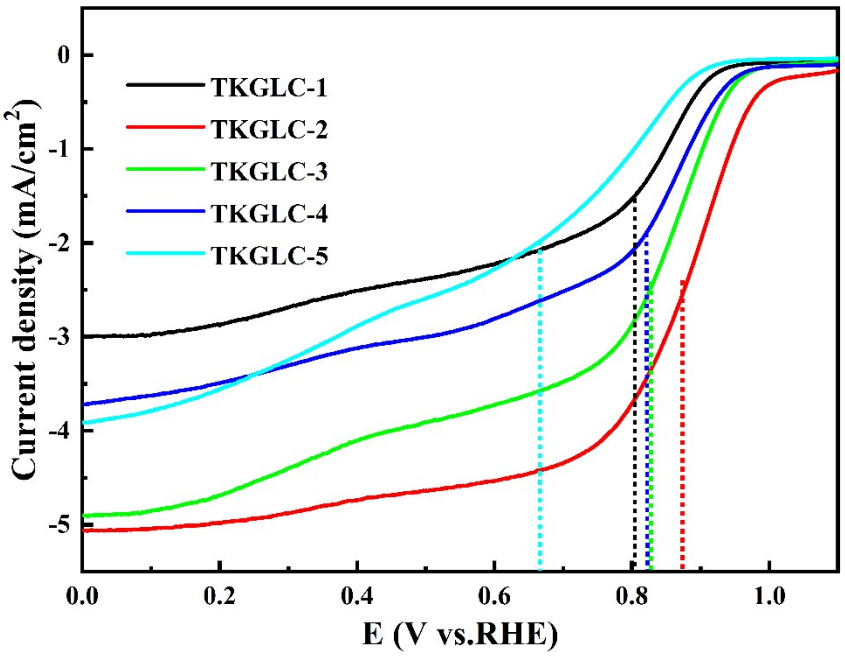

Figure S11. LSV curves of N, S co-doped carbon samples for different mass ratios of thiourea to activated carbon.

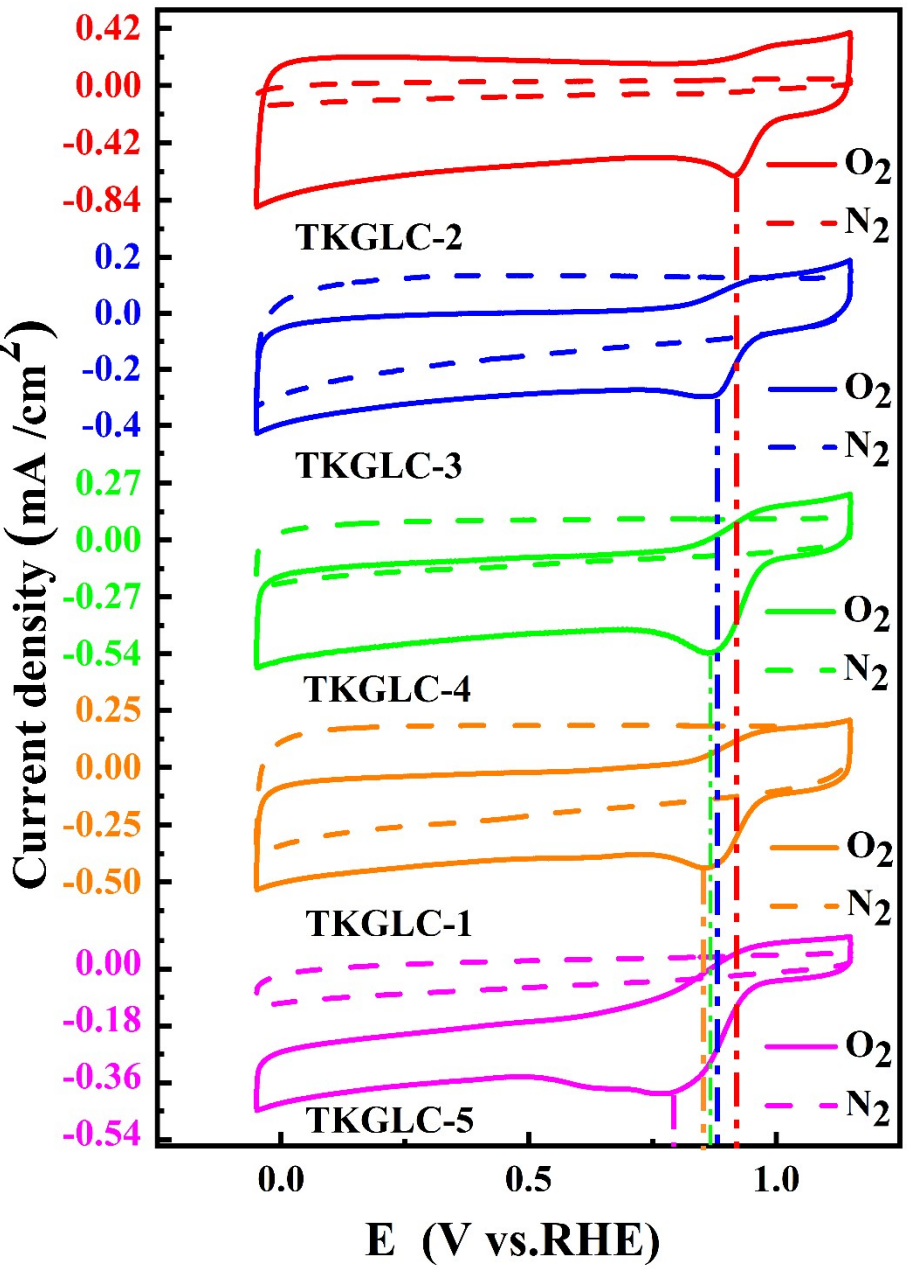

Figure S12. CV curves of N, S co-doped carbon samples for different mass ratios of thiourea to activated carbon in O_2-saturated (solid line) and N_2-saturated (dash line) electrolyte.

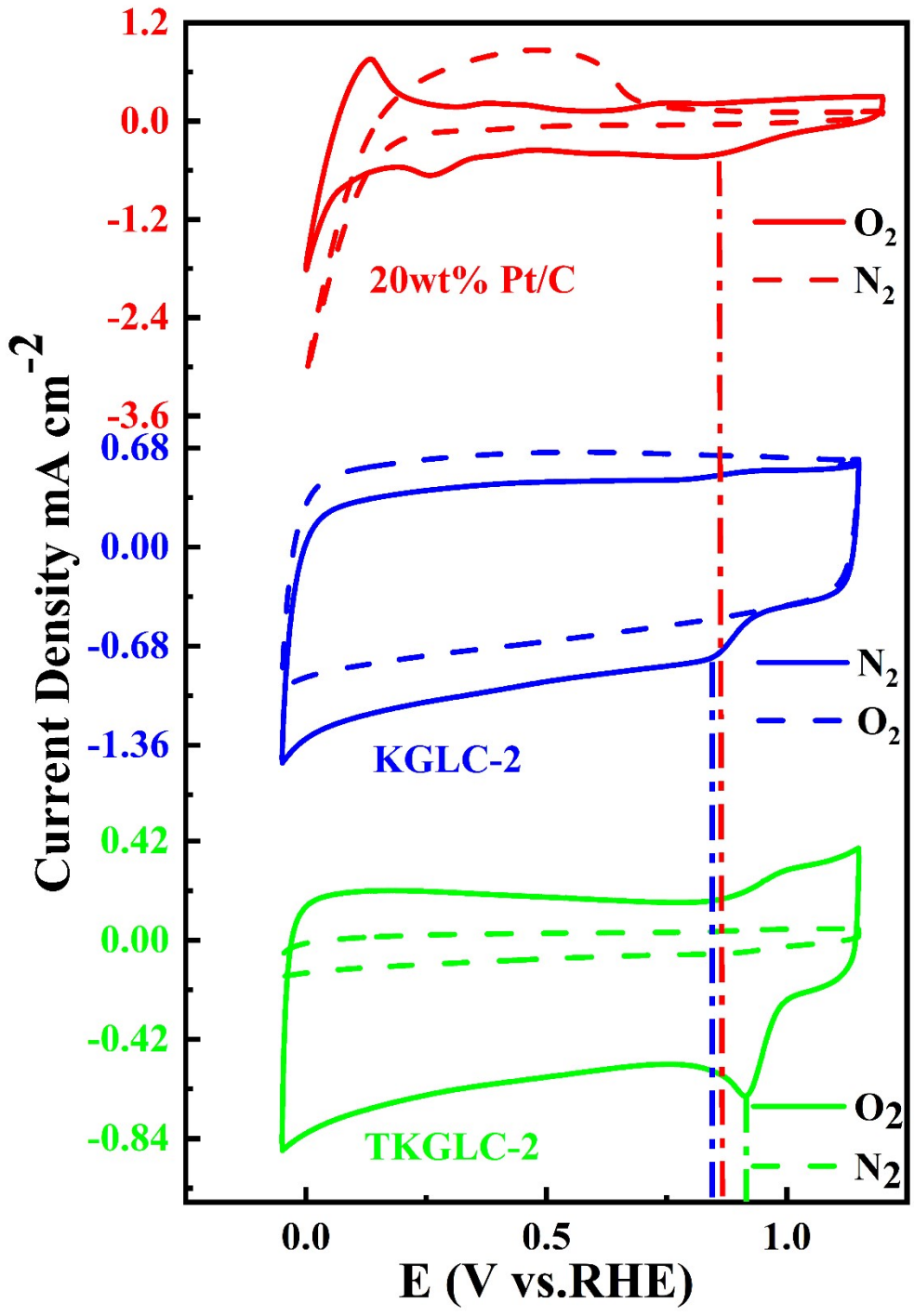

Figure S13. CV curves of different catalysts in O_2-saturated (solid line) and N_2-saturated (dash line) electrolyte.

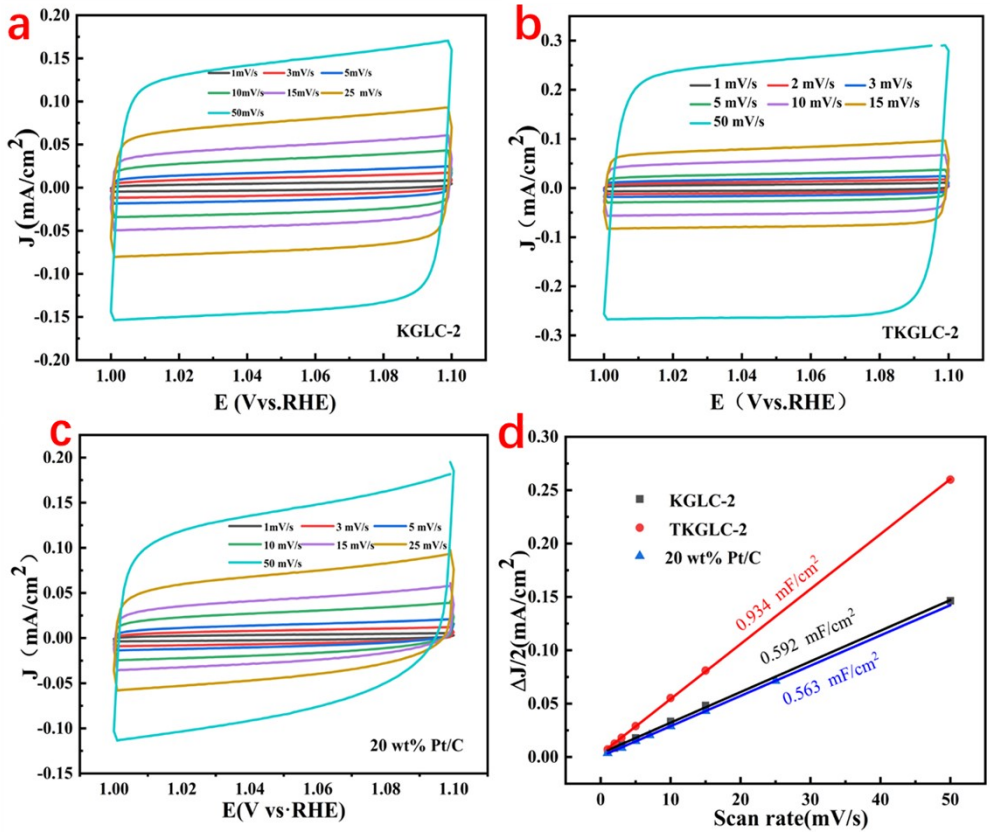

Figure S14. The CV curves for (a) KGLC-2, (b) TKGLC-2, and (c) 20 wt% Pt/C at different scan rates in N_2-saturated 0.1 M KOH solution, (d) Capacitive current density against scan rate.

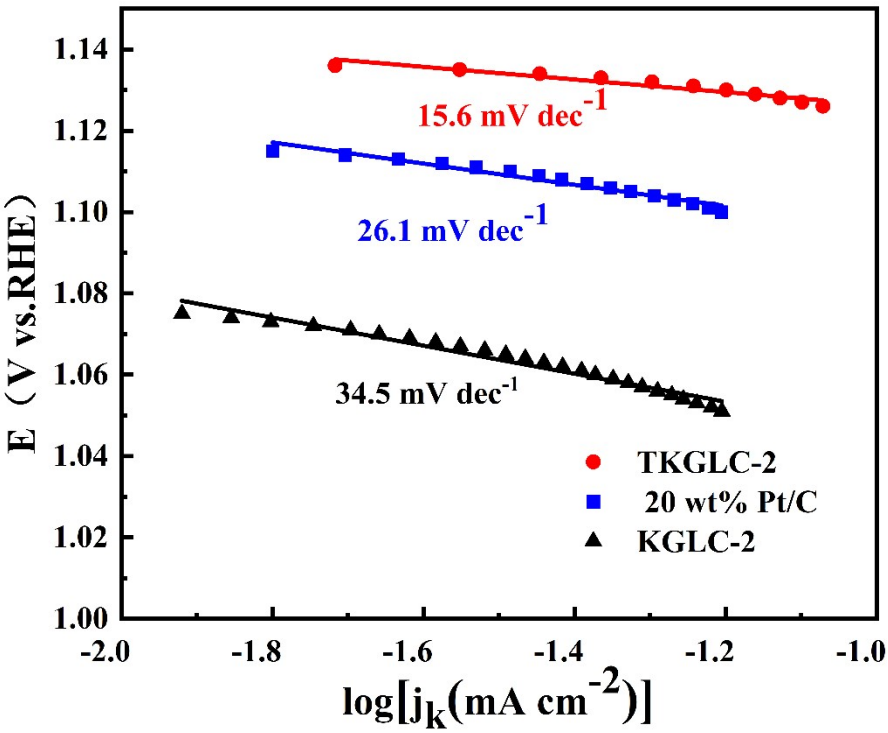

Figure S15. Tafel plots of KGLC-2, TKGLC-2 and 20 wt% Pt/C deriving from the LSVs data

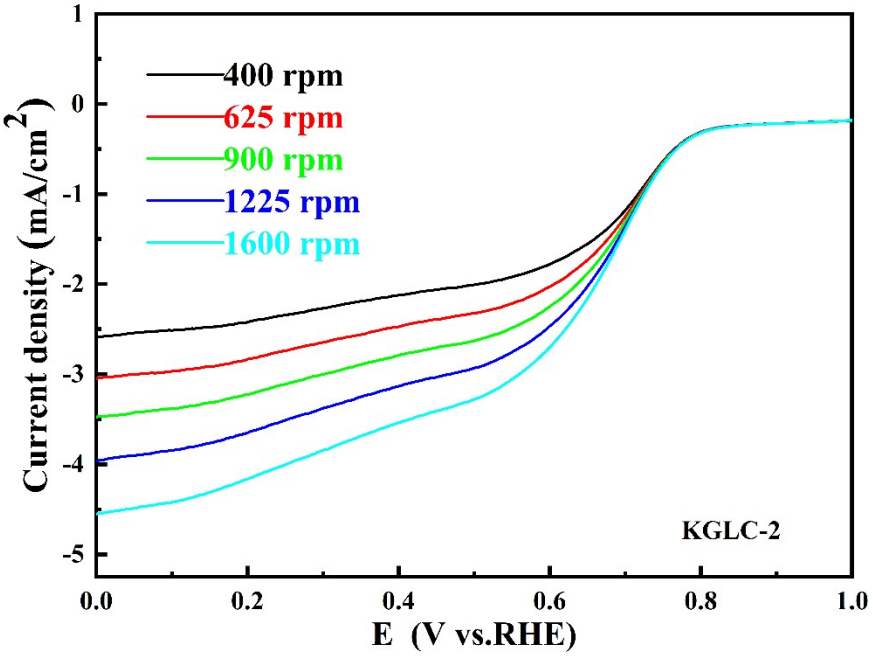

Figure S16. LSV curves of KGLC-2 at different rotation speed (400-1600 rpm) in O_2-saturated electrolyte.

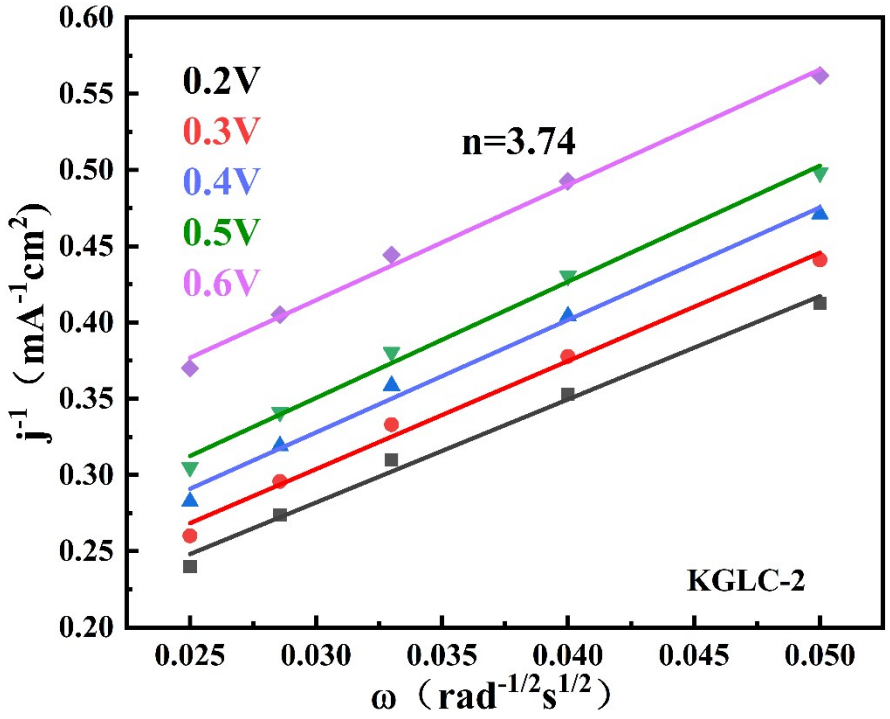

Figure S17. K-L plots of KGLC-2 at different potentials.

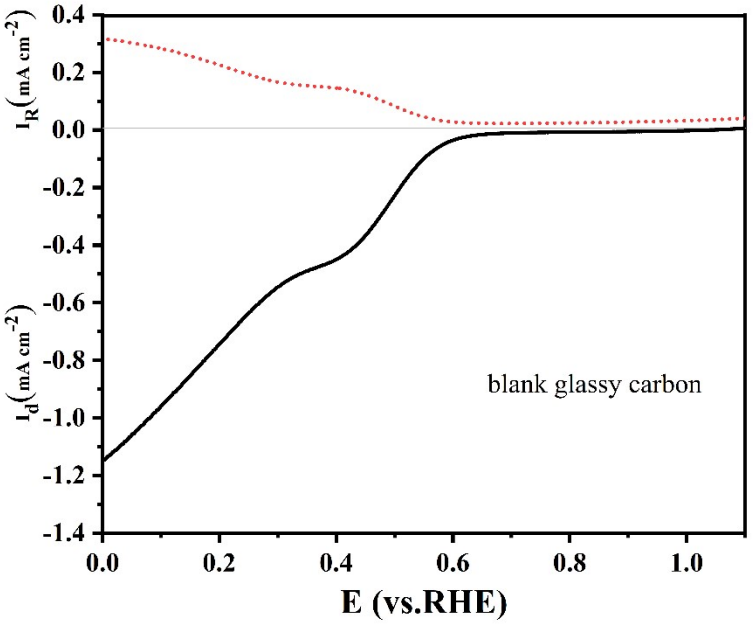

Figure S18. RRDE measurements of the blank glassy carbon in O_2 -saturated 0.1m KOH at 1600 rpm

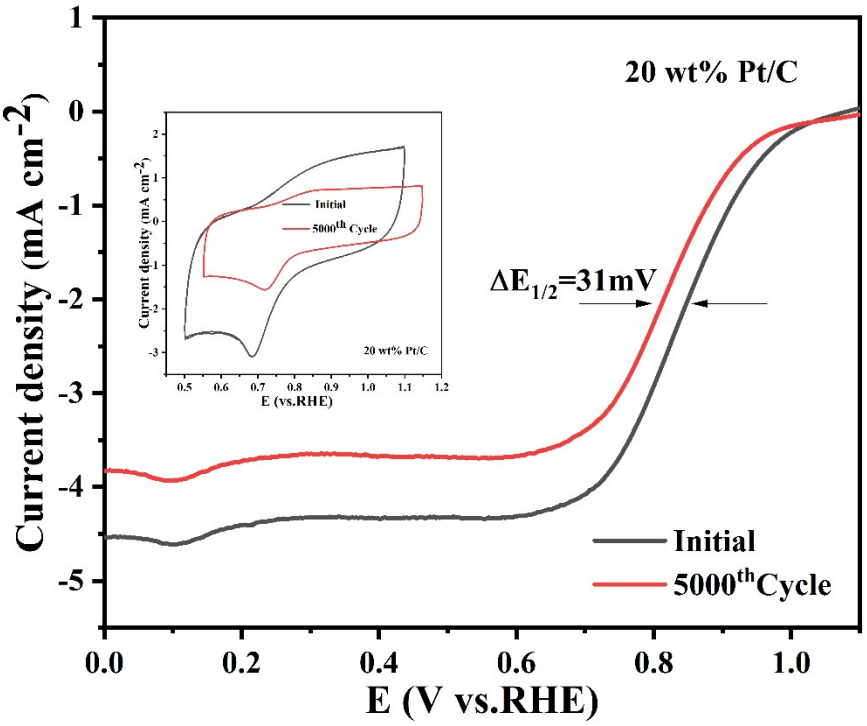

Figure S19. The ORR activity of 20 wt.% Pt/C, measured before and after 5000 cycles. Insets: CVs for ORR at the 20 wt.% Pt/C before cycling and after 5000 cycles.

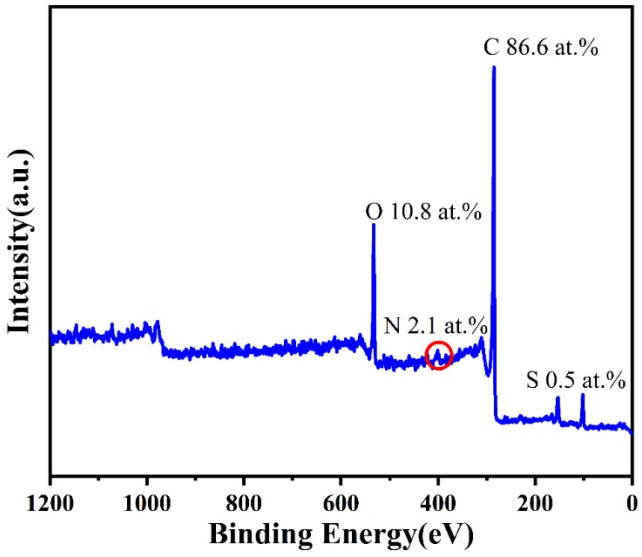

Figure S20. Full XPS spectra of TKGLC-2 catalyst samples.

References

1. K. Liu, X. Ye, A. Zhang, X. Wang, T. Liang, Y. Fang, W. Zhang, K. Hu, X. Liu and X. Chen, *RSC Advance*, 2024, **14**, 5184-5192.
2. K. Liu, X. Huang, H. Wang, F. Li, Y. Tang, J. Li and M. Shao, *ACS Applied Materials & Interfaces*, 2016, **8**, 34422-34430.
3. J. Zhang, M. Tang, X. Sun, N. Huang, Y. Sun, L. Guo and P. Wang, *Journal of Electronic Materials*, 2023, **52**, 2100-2115.
4. Q. Lai, K. Wei, Z. Tang, X. Liu, J. Zheng and Y. Liang, *Journal of Materials Science*, 2021, **56**, 19577-19588.
5. Q. Dong, H. Wang, J. Ren, X. Wang and R. Wang, *Chemical Engineering Journal*, 2022, **442,** 136128-136139.
6. K. K. Hazarika, Y. Yamada, E. V. Matus, M. Kerzhentsev and P. Bharali, *Journal of Power Sources*, 2021, **490**.
7. D. Bhalothia, A. Beniwal, C. Yan, K. Wang, C. Wang and T. Chen, *Chemical Engineering Journal*, 2024, **483**, 149421-149432.
8. T. Getachew, F. Addis, S. Mehretie, H.-L. Yip, R. Xia and S. Admassie, *RSC Advances*, 2020, **10**, 30519-30528.